

1      **MitoChime: A Machine-Learning Pipeline for**  
2      **Detecting PCR-Induced Chimeras in**  
3      **Mitochondrial Illumina Reads**

4                          A Special Project Proposal  
5                          Presented to  
6                          the Faculty of the Division of Physical Sciences and Mathematics  
7                          College of Arts and Sciences  
8                          University of the Philippines Visayas  
9                          Miag-ao, Iloilo

10                         In Partial Fulfillment  
11                         of the Requirements for the Degree of  
12                         Bachelor of Science in Computer Science

13                         by

14                         Duranne Duran  
15                         Yvonne Lin  
16                         Daniella Pailden

17                         Adviser  
18                         Francis D. Dimzon, Ph.D.

19                         December 5, 2025

# **Contents**

21	<b>1 Introduction</b>	1
22	1.1 Overview . . . . .	1
23	1.2 Problem Statement . . . . .	3
24	1.3 Research Objectives . . . . .	4
25	1.3.1 General Objective . . . . .	4
26	1.3.2 Specific Objectives . . . . .	4
27	1.4 Scope and Limitations of the Research . . . . .	5
28	1.5 Significance of the Research . . . . .	6
29	<b>2 Review of Related Literature</b>	7
30	2.1 The Mitochondrial Genome . . . . .	7
31	2.1.1 Mitochondrial Genome Assembly . . . . .	8

32	2.2 PCR Amplification and Chimera Formation . . . . .	9
33	2.3 Existing Traditional Approaches for Chimera Detection . . . . .	10
34	2.3.1 UCHIME . . . . .	11
35	2.3.2 UCHIME2 . . . . .	13
36	2.3.3 CATch . . . . .	14
37	2.3.4 ChimPipe . . . . .	15
38	2.4 Machine Learning Approaches for Chimera and Sequence Quality	
39	Detection . . . . .	16
40	2.4.1 Feature-Based Representations of Genomic Sequences . . .	17
41	2.5 Synthesis of Chimera Detection Approaches . . . . .	18
42	<b>3 Research Methodology</b>	<b>22</b>
43	3.1 Research Activities . . . . .	22
44	3.1.1 Data Collection . . . . .	23
45	3.1.2 Bioinformatics Tools Pipeline . . . . .	27
46	3.1.3 Machine Learning Model Development . . . . .	30
47	3.1.4 Model Benchmarking, Hyperparameter Optimization, and	
48	Evaluation . . . . .	31
49	3.1.5 Feature Importance and Interpretation . . . . .	32

50	3.1.6 Validation and Testing . . . . .	33
51	3.1.7 Documentation . . . . .	34
52	3.2 Calendar of Activities . . . . .	35

# <sup>53</sup> List of Figures

<sup>54</sup>	3.1 Process Diagram of Special Project . . . . .	23
---------------	--	----

# <sup>55</sup> List of Tables

<sup>56</sup>	2.1 Summary of Existing Methods and Research Gaps . . . . .	20
<sup>57</sup>	3.1 Timetable of Activities . . . . .	35

<sup>58</sup> **Chapter 1**

<sup>59</sup> **Introduction**

<sup>60</sup> **1.1 Overview**

<sup>61</sup> The rapid advancement of next-generation sequencing (NGS) technologies has  
<sup>62</sup> transformed genomic research by enabling high-throughput and cost-effective  
<sup>63</sup> DNA analysis (Metzker, 2010). Among current platforms, Illumina sequencing  
<sup>64</sup> remains the most widely adopted, capable of producing millions of short reads  
<sup>65</sup> that can be assembled into reference genomes or analyzed for genetic variation  
<sup>66</sup> (Bentley et al., 2008; Glenn, 2011). Despite its high base-calling accuracy,  
<sup>67</sup> Illumina sequencing is prone to artifacts introduced during library preparation,  
<sup>68</sup> particularly polymerase chain reaction (PCR)-induced chimeras, which are ar-  
<sup>69</sup> tificial hybrid sequences that do not exist in the true genome (Judo, Wedel, &  
<sup>70</sup> Wilson, 1998).

<sup>71</sup> PCR chimeras form when incomplete extension products from one template

72 anneal to an unrelated DNA fragment and are extended, creating recombinant  
73 reads (Qiu et al., 2001). In mitochondrial genome assembly, such artifacts are  
74 especially problematic because the mitochondrial genome is small, circular, and  
75 often repetitive (Boore, 1999; Cameron, 2014). Even a small number of chimeric  
76 or misjoined reads can reduce assembly contiguity and introduce false junctions  
77 during organelle genome reconstruction (Dierckxsens, Mardulyn, & Smits, 2017;  
78 Hahn, Bachmann, & Chevreux, 2013; Jin et al., 2020). Existing assembly tools  
79 such as GetOrganelle and MITObim assume that input reads are largely free of  
80 such artifacts (Hahn et al., 2013; Jin et al., 2020). Consequently, undetected  
81 chimeras may produce fragmented assemblies or misidentified organellar bound-  
82 aries. To ensure accurate reconstruction of mitochondrial genomes, a reliable  
83 method for detecting and filtering PCR-induced chimeras before assembly is es-  
84 sential.

85 This study focuses on mitochondrial sequencing data from the genus *Sar-*  
86 *dinella*, a group of small pelagic fishes widely distributed in Philippine waters.  
87 Among them, *Sardinella lemuru* (Bali sardinella) is one of the country's most  
88 abundant and economically important species, providing protein and livelihood  
89 to coastal communities (Labrador, Agmata, Palermo, Ravago-Gotanco, & Pante,  
90 2021; Willette, Bognot, Mutia, & Santos, 2011). Accurate mitochondrial assem-  
91 blies are critical for understanding its population genetics, stock structure, and  
92 evolutionary history. However, assembly pipelines often encounter errors or fail  
93 to complete due to undetected chimeric reads. To address this gap, this research  
94 introduces MitoChime, a machine learning pipeline designed to detect and filter  
95 PCR-induced chimeric reads using both alignment-based and sequence-derived  
96 statistical features. The tool aims to provide bioinformatics laboratories, partic-

97 ularly the Philippine Genome Center Visayas (PGC Visayas), with an efficient  
98 solution for improving mitochondrial genome reconstruction.

## 99 1.2 Problem Statement

100 While NGS technologies have revolutionized genomic data acquisition, the ac-  
101 curacy of mitochondrial genome assembly remains limited by artifacts produced  
102 during PCR amplification. These chimeric reads can distort assembly graphs and  
103 cause misassemblies, with particularly severe effects in small, circular mitochon-  
104 drial genomes (Boore, 1999; Cameron, 2014). Existing assembly pipelines such  
105 as GetOrganelle, MITObim, and NOVOPlasty assume that sequencing reads are  
106 free of such artifacts (Dierckxsens et al., 2017; Hahn et al., 2013; Jin et al., 2020).  
107 At PGC Visayas, several mitochondrial assemblies have failed or yielded incom-  
108 plete contigs despite sufficient coverage, suggesting that undetected chimeric reads  
109 compromise assembly reliability. Meanwhile, existing chimera detection tools such  
110 as UCHIME and VSEARCH were developed primarily for amplicon-based com-  
111 munity analysis and rely heavily on reference or taxonomic comparisons (Edgar,  
112 Haas, Clemente, Quince, & Knight, 2011; Rognes, Flouri, Nichols, Quince, &  
113 Mahé, 2016). These approaches are unsuitable for single-species organellar data,  
114 where complete reference genomes are often unavailable. Therefore, there is a  
115 pressing need for a reference-independent, data-driven tool capable of detecting  
116 and filtering PCR-induced chimeras in mitochondrial sequencing datasets.

<sub>117</sub> **1.3 Research Objectives**

<sub>118</sub> **1.3.1 General Objective**

<sub>119</sub> This study aims to develop and evaluate a machine learning-based pipeline (Mi-  
<sub>120</sub> toChime) that detects PCR-induced chimeric reads in *Sardinella lemuru* mito-  
<sub>121</sub> chondrial sequencing data in order to improve the quality and reliability of down-  
<sub>122</sub> stream mitochondrial genome assemblies.

<sub>123</sub> **1.3.2 Specific Objectives**

<sub>124</sub> Specifically, the study aims to:

- <sub>125</sub> 1. construct simulated *Sardinella lemuru* Illumina paired-end datasets contain-  
<sub>126</sub> ing both clean and PCR-induced chimeric reads,
- <sub>127</sub> 2. extract alignment-based and sequence-based features such as k-mer compo-  
<sub>128</sub> sition, junction complexity, and split-alignment counts from both clean and  
<sub>129</sub> chimeric reads,
- <sub>130</sub> 3. train, validate, and compare supervised machine-learning models for classi-  
<sub>131</sub> fying reads as clean or chimeric,
- <sub>132</sub> 4. determine feature importance and identify indicators of PCR-induced  
<sub>133</sub> chimerism,
- <sub>134</sub> 5. integrate the optimized classifier into a modular and interpretable pipeline  
<sub>135</sub> deployable on standard computing environments at PGC Visayas.

## <sup>136</sup> 1.4 Scope and Limitations of the Research

<sup>137</sup> This study focuses on detecting PCR-induced chimeric reads in Illumina paired-  
<sup>138</sup> end mitochondrial sequencing data from *Sardinella lemuru*. The decision to re-  
<sup>139</sup> strict the taxonomic scope to a single species is based on four considerations:  
<sup>140</sup> (1) to limit interspecific variation in mitochondrial genome size, GC content, and  
<sup>141</sup> repetitive regions so that differences in read patterns can be attributed more di-  
<sup>142</sup> rectly to PCR-induced chimerism; (2) to align the analysis with relevant *S. lemuru*  
<sup>143</sup> sequencing projects at PGC Visayas; (3) to take advantage of the availability of *S.*  
<sup>144</sup> *lemuru* mitochondrial assemblies and raw datasets in public repositories such as  
<sup>145</sup> the National Center for Biotechnology Information (NCBI), which facilitates refer-  
<sup>146</sup> ence selection and benchmarking; and (4) to develop a tool that directly supports  
<sup>147</sup> local studies on *S. lemuru* population structure and fisheries management.

<sup>148</sup> The study emphasizes `wgsim`-based simulations and selected empirical mito-  
<sup>149</sup> chondrial datasets from *S. lemuru*. It excludes naturally occurring chimeras, nu-  
<sup>150</sup> clear mitochondrial pseudogenes (NUMTs), and large-scale assembly rearrange-  
<sup>151</sup> ments in nuclear genomes. Feature extraction is restricted to low-dimensional  
<sup>152</sup> alignment and sequence statistics, such as k-mer frequency profiles, GC content,  
<sup>153</sup> read length, soft and hard clipping metrics, split-alignment counts, and map-  
<sup>154</sup> ping quality, rather than high-dimensional deep learning embeddings. This de-  
<sup>155</sup> sign keeps model behaviour interpretable and ensures that the pipeline can be  
<sup>156</sup> run on standard workstations at PGC Visayas. Testing on long-read platforms  
<sup>157</sup> (e.g., Nanopore, PacBio) and other taxa is outside the scope of this project; the  
<sup>158</sup> implemented pipeline is evaluated only on short-read *S. lemuru* datasets.

## <sup>159</sup> 1.5 Significance of the Research

<sup>160</sup> This research provides both methodological and practical contributions to mi-  
<sup>161</sup>tochondrial genomics and bioinformatics. First, MitoChime filters PCR-induced  
<sup>162</sup> chimeric reads prior to genome assembly, with the goal of improving the con-  
<sup>163</sup>tiguity and correctness of *Sardinella lemuru* mitochondrial assemblies. Second,  
<sup>164</sup> it replaces informal manual curation with a documented workflow, improving au-  
<sup>165</sup>tomation and reproducibility. Third, the pipeline is designed to run on computing  
<sup>166</sup> infrastructures commonly available in regional laboratories, enabling routine use  
<sup>167</sup> at facilities such as PGC Visayas. Finally, more reliable mitochondrial assemblies  
<sup>168</sup> for *S. lemuru* provide a stronger basis for downstream applications in the field of  
<sup>169</sup> fisheries and genomics.

<sup>170</sup> **Chapter 2**

<sup>171</sup> **Review of Related Literature**

<sup>172</sup> This chapter presents an overview of the literature relevant to the study. It  
<sup>173</sup> discusses the biological and computational foundations underlying mitochondrial  
<sup>174</sup> genome analysis and assembly, as well as existing tools, algorithms, and techniques  
<sup>175</sup> related to chimera detection and genome quality assessment. The chapter aims to  
<sup>176</sup> highlight the strengths, limitations, and research gaps in current approaches that  
<sup>177</sup> motivate the development of the present study.

<sup>178</sup> **2.1 The Mitochondrial Genome**

<sup>179</sup> Mitochondrial genome (mtDNA) is a small, typically circular molecule found in  
<sup>180</sup> most eukaryotes. It encodes essential genes involved in oxidative phosphorylation  
<sup>181</sup> and energy metabolism. Because of its conserved structure, mtDNA has become  
<sup>182</sup> a valuable genetic marker for studies in population genetics and phylogenetics  
<sup>183</sup> (Anderson et al., 1981; Boore, 1999). In animal species, the mitochondrial genome

ranges from 15–20 kilobase and contains 13 protein-coding genes, 22 tRNAs, and two rRNAs arranged compactly without introns (Gray, 2012). In comparison to nuclear DNA, the ratio of the number of copies of mtDNA is higher and has simple organization which make it particularly suitable for genome sequencing and assembly studies (Dierckxsens et al., 2017).

### 2.1.1 Mitochondrial Genome Assembly

Mitochondrial genome assembly refers to the reconstruction of the complete mitochondrial DNA (mtDNA) sequence from raw or fragmented sequencing reads. It is conducted to obtain high-quality, continuous representations of the mitochondrial genome that can be used for a wide range of analyses, including species identification, phylogenetic reconstruction, evolutionary studies, and investigations of mitochondrial diseases. Because mtDNA evolves rapidly, its assembled sequence provides valuable insights into population structure, lineage divergence, and adaptive evolution across taxa (Boore, 1999). Compared to nuclear genome assembly, assembling the mitochondrial genome is often considered more straightforward but still encounters technical challenges such as the formation of chimeric reads. Commonly used tools for mitogenome assembly such as GetOrganelle and MITObim operate under the assumption of organelle genome circularity, and are vulnerable when chimeric reads disrupt this circular structure, resulting in assembly errors (Hahn et al., 2013; Jin et al., 2020).

## 204 2.2 PCR Amplification and Chimera Formation

205 PCR plays an important role in NGS library preparation, as it amplifies target  
206 DNA fragments for downstream analysis. However as previously mentioned, the  
207 amplification process can also introduce chimeric reads which compromises the  
208 quality of the input reads supplied to sequencing or assembly workflows. Chimeras  
209 typically arise when incomplete extension occurs during a PCR cycle. This causes  
210 the DNA polymerase to switch from one template to another and generate hy-  
211 brid recombinant molecules (Judo et al., 1998). Artificial chimeras are produced  
212 through such amplification errors, whereas biological chimeras occur naturally  
213 through genomic rearrangements or transcriptional events.

214 In the context of amplicon-based sequencing, the presence of chimeras can in-  
215 flate estimates of genetic or microbial diversity and may cause misassemblies dur-  
216 ing genome reconstruction. Qin et al. (2023) has reported that chimeric sequences  
217 may account for more than 10% of raw reads in amplicon datasets. This artifact  
218 tends to be most prominent among rare operational taxonomic units (OTUs) or  
219 singletons, which are sometimes misinterpreted as novel diversity, further caus-  
220 ing the complication of microbial diversity analyses (Gonzalez, Zimmermann, &  
221 Saiz-Jimenez, 2004). As such, determining and minimizing PCR-induced chimera  
222 formation is vital for improving the quality of mitochondrial genome assemblies,  
223 and ensuring the reliability of amplicon sequencing data.

224 **2.3 Existing Traditional Approaches for Chimera**

225 **Detection**

226 Several computational tools have been developed to identify chimeric sequences in  
227 NGS datasets. These tools generally fall into two categories: reference-based and  
228 de novo approaches. Reference-based chimera detection, also known as database-  
229 dependent detection, is one of the earliest and most widely used computational  
230 strategies for identifying chimeric sequences in amplicon-based community studies.  
231 These methods rely on the comparison of each query sequence against a curated,  
232 high-quality database of known, non-chimeric reference sequences (Edgar et al.,  
233 2011).

234 On the other hand, the de novo chimera detection, also referred to as reference-  
235 free detection, represents an alternative computational paradigm that identifies  
236 chimeric sequences without reliance on external reference databases. This method  
237 infer chimeras based on internal relationships among the sequences present within  
238 the dataset itself, making it particularly advantageous in studies of under explored  
239 or taxonomically diverse communities where comprehensive reference databases  
240 are unavailable or incomplete (Edgar, 2016; Edgar et al., 2011). The underlying  
241 assumption on this method is that during PCR, true biological sequences are  
242 generally more abundant as they are amplified early and dominate the read pool,  
243 whereas chimeric sequences appear later and are generally less abundant. The  
244 de novo approach leverage this abundance hierarchy, treating the most abundant  
245 sequences as supposed parents and testing whether less abundant sequences can  
246 be reconstructed as mosaics of these templates. Compositional and structural  
247 similarity are also evaluated to check whether different regions of a candidate

248 sequence correspond to distinct high-abundance sequences.

249 In practice, many modern bioinformatics pipelines combine both paradigms  
250 sequentially: an initial de novo step identifies dataset-specific chimeras, followed  
251 by a reference-based pass that removes remaining artifacts relative to established  
252 databases (Edgar, 2016). These two methods of detection form the foundation of  
253 tools such as UCHIME and later UCHIME2.

### 254 2.3.1 UCHIME

255 Developed by Edgar et al. (Edgar et al., 2011), UCHIME is one of the most widely  
256 used computational tools for detecting chimeric sequences in amplicon sequencing  
257 data. The UCHIME algorithm detects chimeras by evaluating how well a query  
258 sequence ( $Q$ ) can be explained as a mosaic of two parent sequences ( $A$  and  $B$ )  
259 from a reference database. The query sequence is first divided into four non-  
260 overlapping segments or chunks. Each chunk is independently searched against a  
261 reference database that is assumed to be free of chimeras. The best matches to  
262 each segment are collected, and from these results, two candidate parent sequences  
263 are identified, typically the two sequences that best explain all chunks of the query.  
264 Then a three-way alignment among the query ( $Q$ ) and the two parent candidates  
265 ( $A$  and  $B$ ) is done. From this alignment, UCHIME attempts to find a chimeric  
266 model ( $M$ ) which is a hypothetical recombinant sequence formed by concatenating  
267 fragments from  $A$  and  $B$  that best match the observed  $Q$

268 **Chimeric Alignment and Scoring**

269 To decide whether a query is chimeric, UCHIME computes several alignment-  
270 based metrics between Q, its top hit (T, the most similar known sequence), and  
271 the chimeric model (M). The key differences are measured as: dQT or the number  
272 of mismatches between the query and the top hit as well as dQM or the number  
273 of mismatches between the query and the chimeric model. From these, a chimera  
274 score is calculated to quantify how much better the chimeric model fits the query  
275 compared to a single parent. If the model's similarity to Q exceeds a defined  
276 threshold (typically  $\geq 0.8\%$  better identity), the sequence is reported as chimeric.  
277 A higher score indicates stronger evidence of chimerism, while lower scores suggest  
278 that the sequence is more likely to be authentic.

279 In de novo mode, UCHIME applies an abundance-driven strategy. Only se-  
280 quences at least twice as abundant as the query are considered as potential parents.  
281 Non-chimeric sequences identified at each step are added iteratively to a growing  
282 internal database for subsequent queries.

283 **Limitations of UCHIME**

284 Although UCHIME was a significant advancement in chimera detection, it has  
285 notable limitations. According to (Edgar, 2016) and the UCHIME practical notes  
286 (Edgar, n.d), many of the accuracy results reported in the original 2011 paper  
287 were overly optimistic due to unrealistic benchmark designs that assumed com-  
288 plete reference coverage and perfect sequence quality. In practice, UCHIME's  
289 accuracy can decline when (1) the reference database is incomplete or contains

290 erroneous entries; (2) low-divergence chimeras are present, as these closely resem-  
291 ble genuine biological variants; (3) sequence datasets include residual sequencing  
292 errors, leading to spurious alignments or misidentification; and (4) the abundance  
293 ratio between parent and chimera is distorted by amplification bias. Additionally,  
294 UCHIME tends to misclassify sequences as non-chimeric when parent sequences  
295 are missing from the database. These limitations motivated the development of  
296 UCHIME2.

### 297 **2.3.2 UCHIME2**

298 To overcome the limitations of its predecessor, UCHIME2 (Edgar, 2016) intro-  
299 duced several methodological and algorithmic refinements that significantly en-  
300 hanced the accuracy and reliability of chimera detection. One major improve-  
301 ment lies in its approach to uncertainty handling. In earlier versions, sequences  
302 with limited reference support were often incorrectly classified as non-chimeric,  
303 increasing the likelihood of false negatives. UCHIME2 addresses this issue by  
304 designating such ambiguous sequences as “unknown,” thereby providing a more  
305 conservative and reliable classification framework.

306 Another notable advancement is the introduction of multiple application-  
307 specific modes that allow users to tailor the algorithm’s performance to the  
308 characteristics of their datasets. The following parameter presets: denoised,  
309 balanced, sensitive, specific, and high-confidence, enable researchers to optimize  
310 the balance between sensitivity and specificity according to the goals of their  
311 analysis.

312 In comparative evaluations, UCHIME2 demonstrated superior detection per-  
313 formance, achieving sensitivity levels between 93% and 99% and lower overall  
314 error rates than earlier versions or other contemporary tools such as DECIPHER  
315 and ChimeraSlayer. Despite these advances, the study also acknowledged a fun-  
316 damental limitation in chimera detection: complete error-free identification is  
317 theoretically unattainable. This is due to the presence of “perfect fake models,”  
318 wherein genuine non-chimeric sequences can be perfectly reconstructed from other  
319 reference fragments. This underscore the uncertainty in differentiating authentic  
320 biological sequences from artificial recombinants based solely on sequence similar-  
321 ity, emphasizing the need for continued methodological refinement and cautious  
322 interpretation of results.

### 323 2.3.3 CATch

324 As previously mentioned, UCHIME (Edgar et al., 2011) relied on alignment-based  
325 sequences in amplicon data. However, researchers soon observed that different al-  
326 gorithms often produced inconsistent predictions. A sequence might be identified  
327 as chimeric by one tool but classified as non-chimeric by another, resulting in  
328 unreliable filtering outcomes across studies.

329 To address these inconsistencies, Mysara, Saeys, Leys, Raes, and Monsieurs  
330 (2015) developed the Classifier for Amplicon Tool Chimeras (CATCh), which rep-  
331 resents the first ensemble machine learning system designed for chimera detection  
332 in 16S rRNA amplicon sequencing. Rather than depending on a single detec-  
333 tion strategy, CATCh integrates the outputs of several established tools, includ-  
334 ing UCHIME, ChimeraSlayer, DECIPHER, Pintail, and Perseus. The individual

335 scores and binary decisions generated by these tools are used as input features for  
336 a supervised learning model. The algorithm employs a Support Vector Machine  
337 (SVM) with a Pearson VII Universal Kernel (PUK) to determine optimal weight-  
338 ings among the input features and to assign each sequence a probability of being  
339 chimeric.

340 Benchmarking in both reference-based and de novo modes demonstrated signif-  
341 icant performance improvements. CATCh achieved sensitivities of approximately  
342 85 percent in reference-based mode and 92 percent in de novo mode, with corre-  
343 sponding specificities of approximately 96 percent and 95 percent. These results  
344 indicate that CATCh detected 7 to 12 percent more chimeras than any individual  
345 algorithm while maintaining high precision.

### 346 2.3.4 ChimPipe

347 Among the available tools for chimera detection, ChimPipe is a pipeline developed  
348 to identify chimeric sequences such as biological chimeras. It uses both discordant  
349 paired-end reads and split-read alignments to improve the accuracy and sensitivity  
350 of detecting biological chimeras (Rodriguez-Martin et al., 2017). By combining  
351 these two sources of information, ChimPipe achieves better precision than meth-  
352 ods that depend on a single type of indicator.

353 The pipeline works with many eukaryotic species that have available genome  
354 and annotation data (Rodriguez-Martin et al., 2017). It can also predict multiple  
355 isoforms for each gene pair and identify breakpoint coordinates that are useful  
356 for reconstructing and verifying chimeric transcripts. Tests using both simulated

357 and real datasets have shown that ChimPipe maintains high accuracy and reliable  
358 performance.

359 ChimPipe lets users adjust parameters to fit different sequencing protocols or  
360 organism characteristics. Experimental results have confirmed that many chimeric  
361 transcripts detected by the tool correspond to functional fusion proteins, demon-  
362 strating its utility for understanding chimera biology and its potential applications  
363 in disease research (Rodriguez-Martin et al., 2017).

## 364 **2.4 Machine Learning Approaches for Chimera 365 and Sequence Quality Detection**

366 Traditional chimera detection tools rely primarily on heuristic or alignment-based  
367 rules. Recent advances in machine learning (ML) have demonstrated that models  
368 trained on sequence-derived features can effectively capture compositional and  
369 structural patterns in biological sequences. Although most existing ML systems  
370 such as those used for antibiotic resistance prediction, taxonomic classification,  
371 or viral identification are not specifically designed for chimera detection, they  
372 highlight how data-driven models can outperform similarity-based heuristics by  
373 learning intrinsic sequence signatures. In principle, ML frameworks can integrate  
374 indicators such as k-mer frequencies, GC-content variation and split-alignment  
375 metrics to identify subtle anomalies that may indicate a chimeric origin (Arango  
376 et al., 2018; Liang, Bible, Liu, Zou, & Wei, 2020; Ren et al., 2020).

### **377 2.4.1 Feature-Based Representations of Genomic Se- 378 quences**

In genomic analysis, feature extraction converts DNA sequences into numerical representations suitable for ML algorithms. A common approach is k-mer frequency analysis, where normalized k-mer counts form the feature vector (Vervier, Mahé, Tournoud, Veyrieras, & Vert, 2015). These features effectively capture local compositional patterns that often differ between authentic and chimeric reads.

In particular, deviations in k-mer profiles between adjacent read segments can serve as a compositional signature of template-switching events. Additional descriptors such as GC content and sequence entropy can further distinguish sequence types; in metagenomic classification and virus detection, k-mer-based features have shown strong performance and robustness to noise (Ren et al., 2020; Vervier et al., 2015). For chimera detection specifically, abrupt shifts in GC or k-mer composition along a read can indicate junctions between parental fragments. Windowed feature extraction enables models to capture these discontinuities that rule-based algorithms may overlook.

Machine learning models can also leverage alignment-derived features such as the frequency of split alignments, variation in mapping quality, and local coverage irregularities. Split reads and discordant read pairs are classical indicators of genomic junctions and have been formalized in probabilistic frameworks for structural-variant discovery that integrate multiple evidence types (Layer, Hall, & Quinlan, 2014). Similarly, long-read tools such as Sniffles employ split-alignment and coverage anomalies to accurately localize breakpoints (Sedlazeck et al., 2018). Modern aligners such as Minimap2 (Li, 2018) output supplementary (SA tags) and

401 secondary alignments as well as chaining and alignment-score statistics that can  
402 be summarized into quantitative predictors for machine-learning models. These  
403 alignment-signal features are particularly relevant to PCR-induced mitochondrial  
404 chimeras, where template-switching events produce reads partially matching dis-  
405 tinct regions of the same or related genomes. Integrating such cues within a  
406 supervised-learning framework enables artifact detection even in datasets lacking  
407 complete or perfectly assembled references.

408 A further biologically grounded descriptor is the length of microhomology at  
409 putative junctions. Microhomology refers to short, shared sequences, often in the  
410 range of a few to tens of base pairs that are near breakpoints where template-  
411 switching events typically happen. Studies of double strand break repair and  
412 structural variation have demonstrated that the length of microhomology corre-  
413 lates with the likelihood of microhomology-mediated end joining (MMEJ) or fork-  
414 stalled template-switching pathways (Sfeir & Symington, 2015). In the context of  
415 PCR-induced chimeras, template switching during amplification often leaves short  
416 identical sequences at the junction of two concatenated fragments. Quantifying  
417 the longest exact suffix-prefix overlap at each candidate breakpoint thus provides  
418 a mechanistic signature of chimerism and complements both compositional (k-  
419 mer) and alignment (SA count) features.

## 420 2.5 Synthesis of Chimera Detection Approaches

421 To provide an integrated overview of the literature discussed in this chapter, Ta-  
422 ble 2.1 summarizes the major chimera detection studies, their methodological

<sup>423</sup> approaches, and their known limitations.

Table 2.1: Summary of Existing Methods and Research Gaps

Method/Study	Scope/Approach	Limitations
Reference-based Chimera Detection	Compares query sequences against curated, non-chimeric reference databases; identifies mosaic sequences by evaluating similarity to known templates.	Depends heavily on completeness and quality of reference databases; often fails when novel taxa or missing parent sequences are present; reduced accuracy for low-divergence chimeras.
De novo Chimera Detection	Identifies chimeras using only internal dataset relationships; relies on abundance patterns and compositional similarity; reconstructs sequences as mosaics of high-abundance parents.	Assumes true sequences are more abundant—fails when amplification bias distorts abundance; struggles with evenly abundant parental sequences; can misclassify highly similar true variants.
UCHIME	Alignment-based chimera detection; segments query sequence, identifies parent candidates, performs 3-way alignment, and computes chimera scores; supports both reference-based and de novo modes.	Accuracy inflated in original benchmarks; suffers under incomplete databases; poor performance on low-divergence chimeras; sensitive to sequencing errors; misclassifies when parents are missing.
UCHIME2	Improved uncertainty handling; classifies ambiguous sequences as unknown; offers multiple sensitivity/specificity modes; more robust with incomplete references; higher sensitivity (93–99%).	Cannot achieve perfect accuracy due to “perfect fake models”; genuine variants may be indistinguishable from artificial recombinants; theoretical detection limit remains.
CATCh	First ML ensemble tool for 16S chimera detection; integrates outputs of UCHIME, ChimeraSlayer, DECIPHER, Pintail, Perseus via SVM classifier; significantly improves sensitivity and specificity.	Depends on performance of underlying tools; ML model limited to features they output; ensemble can still misclassify in datasets with extreme novelty or low coverage.
ChimPipe	Pipeline for detecting fusion genes and transcript-derived chimeras in	Designed for RNA-seq, not amplicons; needs high-quality genome

424 Across existing studies, no single approach reliably detects all forms of chimeric  
425 sequences, particularly those generated by PCR-induced template switching in  
426 mitochondrial genomes. Reference-based tools perform poorly when parental se-  
427 quences are absent; de novo methods rely strongly on abundance assumptions;  
428 alignment-based systems show reduced sensitivity to low-divergence chimeras; and  
429 ensemble methods inherit the limitations of their component algorithms. RNA-  
430 seq-oriented pipelines likewise do not generalize well to organelle data. Although  
431 machine learning approaches offer promising feature-based detection, they are  
432 rarely applied to mitochondrial genomes and are not trained specifically on PCR-  
433 induced organelle chimeras. These limitations indicate a clear research gap: the  
434 need for a specialized, feature-driven classifier tailored to mitochondrial PCR-  
435 induced chimeras that integrates k-mer composition, split-alignment signals, and  
436 micro-homology features to achieve more accurate detection than current heuristic  
437 or alignment-based tools.

<sup>438</sup> **Chapter 3**

<sup>439</sup> **Research Methodology**

<sup>440</sup> This chapter outlines the steps involved in completing the study, including data  
<sup>441</sup> gathering, generating simulated mitochondrial Illumina reads, preprocessing and  
<sup>442</sup> indexing the data, developing a bioinformatics pipeline to extract key features,  
<sup>443</sup> applying machine learning algorithms for chimera detection, and validating and  
<sup>444</sup> comparing model performance.

<sup>445</sup> **3.1 Research Activities**

<sup>446</sup> As illustrated in Figure 3.1, this study carried out a sequence of procedures to  
<sup>447</sup> detect PCR-induced chimeric reads in mitochondrial genomes. The process began  
<sup>448</sup> with collecting a mitochondrial reference sequence of *Sardinella lemuru* from the  
<sup>449</sup> National Center for Biotechnology Information (NCBI) database, which was used  
<sup>450</sup> as a reference for generating simulated clean and chimeric reads. These reads  
<sup>451</sup> were subsequently indexed and mapped. The resulting collections then passed

452 through a bioinformatics pipeline that extracted k-mer profiles, supplementary  
453 alignment (SA) features, and microhomology information to prepare the data for  
454 model construction. The machine learning model was trained using the processed  
455 input, and its precision and accuracy were assessed. It underwent tuning until it  
456 reached the desired performance threshold, after which it proceeded to validation  
457 and will undergo testing.

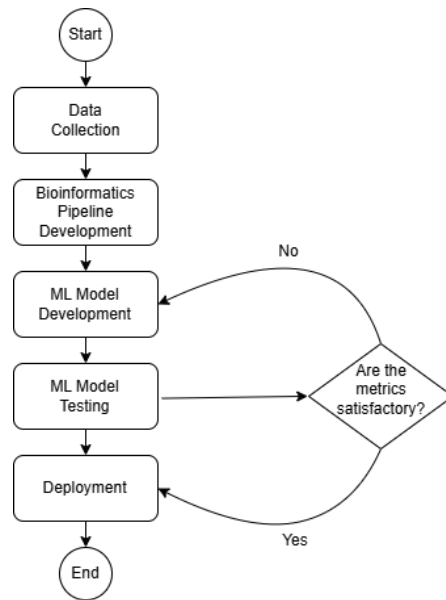


Figure 3.1: Process Diagram of Special Project

### 458 3.1.1 Data Collection

459 The mitochondrial genome reference sequence of *S. lemuru* was obtained from the  
460 NCBI database (accession number NC\_039553.1) in FASTA format. This sequence  
461 served as the basis for generating simulated reads for model development.

462 This step was scheduled to begin in the first week of November 2025 and  
463 expected to be completed by the end of that week, with a total duration of ap-

464 proximately one (1) week.

## 465 Data Preprocessing

466 To reduce manual repetition, all steps in the simulation and preprocessing pipeline  
467 were executed using a custom script in Python (Version 3.11). The script runs  
468 each stage, including read simulation, reference indexing, mapping, and alignment  
469 processing, in a fixed sequence.

470 Sequencing data were simulated from the NCBI reference genome using `wgsim`  
471 (Version 1.13). First, a total of 10,000 paired-end fragments were simulated,  
472 producing 20,000 reads (10,000 forward and 10,000 reverse) from the the original  
473 reference (`original_reference.fasta`) and and designated as clean reads using  
474 the command:

```
475 wgsim -1 150 -2 150 -r 0 -R 0 -X 0 -e 0.001 -N 10000 \  
476     original_reference.fasta ref1.fastq ref2.fastq
```

477 The command parameters are as follows:

- 478 • `-1` and `-2`: read lengths of 150 base pairs for each paired-end read.
- 479 • `-r`, `-R`, `-X`: mutation rate, fraction of indels, and indel extension probability,  
480 all set to a default value of 0.
- 481 • `-e`: base error rate, set to 0.001 to simulate realistic sequencing errors.
- 482 • `-N`: number of read pairs, set to 10,000.

483 Chimeric sequences were then generated from the same NCBI reference using a  
484 separate Python script. Two non-adjacent segments were randomly selected such  
485 that their midpoint distances fell within specified minimum and maximum thresh-  
486 olds. The script attempts to retain microhomology, or short identical sequences  
487 at segment junctions, to mimic PCR-induced template switching. The resulting  
488 chimeras were written to `chimera_reference.fasta`, with headers recording seg-  
489 ment positions and microhomology length. The `chimera_reference.fasta` was  
490 processed with `wgsim` to simulate 10,000 paired-end fragments, generating 20,000  
491 chimeric reads (10,000 forward reads in `chimeric1.fastq` and 10,000 reverse reads  
492 in `chimeric2.fastq`) using the command format.

493 Next, a `minimap2` index of the reference genome was created using:

```
494 minimap2 -d ref.mmi original_reference.fasta
```

495 Minimap2 (Version 2.28) is a tool used to map reads to a reference genome.  
496 The index `ref.mmi` of the original reference sequence is required by `minimap2` for  
497 efficient read mapping. Mapping allows extraction of alignment features from each  
498 read, which were used as input for the machine learning model. The simulated  
499 clean and chimeric reads were then mapped to the reference index as follows:

```
500 minimap2 -ax sr -t 8 ref.mmi ref1.fastq ref2.fastq > clean.sam
```

```
501 minimap2 -ax sr -t 8 ref.mmi \  
502 chimeric1.fastq chimeric2.fastq > chimeric.sam
```

503 Here, `-ax sr` specifies short-read alignment mode, and `-t 8` uses 8 CPU

504 threads. The resulting clean and chimeric SAM files contain the alignment posi-  
505 tions of each read relative to the original reference genome.

506 The SAM files were then converted to BAM format, sorted, and indexed using  
507 `samtools` (Version 1.20):

```
508 samtools view -bS clean.sam -o clean.bam  
509 samtools view -bS chimeric.sam -o chimeric.bam  
510  
511 samtools sort clean.bam -o clean.sorted.bam  
512 samtools index clean.sorted.bam  
513  
514 samtools sort chimeric.bam -o chimeric.sorted.bam  
515 samtools index chimeric.sorted.bam
```

516 BAM files are the compressed binary version of SAM files, which enables faster  
517 processing and reduced storage. Sorting arranges reads by genomic coordinates,  
518 and indexing allows detection of SA as a feature for the machine learning model.

519 The total number of simulated reads was expected to be 40,000. The final col-  
520 lection of reads contained 19,984 clean reads and 20,000 chimeric reads (39,984 en-  
521 tries in total), providing a roughly balanced distribution between the two classes.  
522 After alignment with `minimap2`, only 19,984 clean reads remained because un-  
523 mapped reads were not included in the BAM file. Some sequences failed to align  
524 due to the 5% error rate defined during `wgsim` simulation, which produced mis-  
525 matches that caused certain reads to fall below the aligner's matching threshold.

526 This whole process is scheduled to start in the second week of November 2025

527 and is expected to be completed by the last week of November 2025, with a total  
528 duration of approximately three (3) weeks.

### 529 **3.1.2 Bioinformatics Tools Pipeline**

530 A bioinformatics pipeline will be developed and implemented to extract the neces-  
531 sary analytical features. This pipeline will function as a reproducible and modular  
532 workflow that accepts FASTQ and BAM/SAM file inputs, processes them using  
533 tools such as `samtools` and `jellyfish` (Version 2.3.1), and produces tabular fea-  
534 ture matrices (TSV) for downstream machine learning. To ensure correctness  
535 and adherence to best practices, bioinformatics experts at the PGC Visayas will  
536 be consulted to validate the pipeline design, feature extraction logic, and overall  
537 data integrity. This stage of the study is scheduled to begin in the first week of  
538 January 2026 and conclude by the last week of February 2026, with an estimated  
539 total duration of approximately two (2) months.

540 The bioinformatics pipeline focuses on three principal features from the simu-  
541 lated and aligned sequencing data: (1) supplementary alignment flag (SA count),  
542 (2) k-mer composition difference between read segments, and (3) microhomology  
543 length at potential junctions. Each of these features captures a distinct biological  
544 or computational signature associated with PCR-induced chimeras.

#### 545 **Supplementary Alignment Flag**

546 Supplementary alignment information will be assessed using the mapped and  
547 sorted BAM files (`clean.sorted.bam` and `chimeric.sorted.bam`) generated

548 from the data preprocessing stage. Alignment summaries will be checked using  
549 `samtools flagstat` to obtain preliminary quality-control statistics, including  
550 counts of primary, secondary, and supplementary (SA) alignments.

551 Both BAM files will be converted to SAM format for detailed inspection of  
552 reads in each file:

```
553 samtools view -h clean.sorted.bam -o clean.sorted.sam  
554 samtools view -h chimeric.sorted.bam -o chimeric.sorted.sam
```

555 The SAM output will be checked for reads containing the SA:Z flag, as it  
556 denotes supplementary alignments. Reads exhibiting these or substantial soft-  
557 clipped regions will be considered strong candidates for chimeric artifacts. A  
558 custom Python script would be created to extract the alignment-derived features  
559 and relevant metadata including mapping quality, SAM flag information, CIGAR-  
560 based clipping, and alignment coordinates. These extracted attributes would then  
561 be organized and compiled into a TSV (.tsv) file.

## 562 K-mer Composition Difference

563 Chimeric reads often comprise fragments from distinct genomic regions, resulting  
564 in a compositional discontinuity between segments. Comparing k-mer frequency  
565 profiles between the left and right halves of a read allows detection of such abrupt  
566 compositional shifts, independent of alignment information. This will be obtained  
567 using Jellyfish, a fast k-mer counting software. For each read, the sequence will  
568 be divided into two segments, either at the midpoint or at empirically determined  
569 breakpoints inferred from supplementary alignment data, to generate left and right

570 sequence segments. Jellyfish will then compute k-mer frequency profiles (with  $k =$   
571 5 or 6) for each segment. The resulting k-mer frequency vectors will be normalized  
572 and compared using distance metrics such as cosine similarity or Jensen–Shannon  
573 divergence to quantify compositional disparity between the two halves of the same  
574 read. The resulting difference scores will be stored in a structured TSV file.

## 575 Micro-homology Length

576 The micro-homology length will be computed using a custom Python script that  
577 detects the longest exact suffix–prefix overlap within  $\pm 30$  base pairs surround-  
578 ing a candidate breakpoint. This analysis identifies the number of consecutive  
579 bases shared between the end of one segment and the beginning of another. The  
580 presence and length of such micro-homology are classic molecular signatures of  
581 PCR-induced template switching, where short identical regions (typically 3–15  
582 base pairs) promote premature termination and recombination of DNA synthesis  
583 on a different template strand. Quantifying micro-homology allows assessment of  
584 whether the suspected breakpoint reflects PCR artifacts or true biological variants.  
585 Each read will therefore be annotated with its corresponding micro-homology  
586 length, overlap sequence, and GC content.

587 After extracting the three primary features, all resulting TSV files will be  
588 joined using the read identifier as a common key to generate a unified feature ma-  
589 trix. Additional read-level metadata such as read length, mean base quality, and  
590 number of clipped bases will also be included to provide contextual information.  
591 This consolidated dataset will serve as the input for subsequent machine-learning  
592 model development and evaluation.

593     3.1.3 Machine Learning Model Development

594     After feature extraction, the per-read feature matrices for clean and chimeric  
595     reads were merged into a single dataset. Each row corresponded to one paired-  
596     end read, and columns encoded alignment-structure features (e.g., supplementary  
597     alignment count and spacing between segments), CIGAR-derived soft-clipping  
598     statistics (e.g., left and right soft-clipped length, total clipped bases), k-mer com-  
599     position discontinuity between read segments, and microhomology descriptors  
600     near candidate junctions. The resulting feature set was restricted to quantities  
601     that can be computed from standard BAM/FASTQ files in typical mitochondrial  
602     sequencing workflows.

603       The labelled dataset was randomly partitioned into training (80%) and test  
604       (20%) subsets using stratified sampling to preserve the 1:1 ratio of clean to  
605       chimeric reads. Model development and evaluation were implemented in Python  
606       (Version 3.11) using the `scikit-learn`, `xgboost`, `lightgbm`, and `catboost` li-  
607       braries. A broad panel of classification algorithms was then benchmarked on the  
608       training data to obtain a fair comparison of different model families under identical  
609       feature conditions. The panel included: a trivial dummy classifier, L2-regularized  
610       logistic regression, a calibrated linear support vector machine (SVM),  $k$ -nearest  
611       neighbours, Gaussian Naïve Bayes, decision-tree ensembles (Random Forest, Ex-  
612       tremely Randomized Trees, and Bagging with decision trees), gradient boosting  
613       methods (Gradient Boosting, XGBoost, LightGBM, and CatBoost), and a shallow  
614       multilayer perceptron (MLP).

615       For each model, five-fold stratified cross-validation was performed on the train-  
616       ing set. In every fold, four-fifths of the data were used for fitting and the remaining

617 one-fifth for validation. Mean cross-validation accuracy, precision, recall, F1-score  
618 for the chimeric class, and area under the receiver operating characteristic curve  
619 (ROC–AUC) were computed to summarize performance and rank candidate meth-  
620 ods. This baseline screen allowed comparison of linear, probabilistic, neural, and  
621 ensemble-based approaches and identified tree-based ensemble and boosting mod-  
622 els as consistently strong performers relative to simpler baselines.

623 **3.1.4 Model Benchmarking, Hyperparameter Optimiza-  
624 tion, and Evaluation**

625 Model selection and refinement proceeded in two stages. First, the cross-validation  
626 results from the broad panel were used to identify a subset of competitive mod-  
627 els for more detailed optimization. Specifically, ten model families were carried  
628 forward: L2-regularized logistic regression, calibrated linear SVM, Random For-  
629 est, ExtraTrees, Gradient Boosting, XGBoost, LightGBM, CatBoost, Bagging  
630 with decision trees, and a shallow MLP. This subset spans both linear and non-  
631 linear decision boundaries, but emphasizes ensemble and boosting methods, which  
632 showed superior F1 and ROC–AUC in the initial benchmark.

633 Second, hyperparameter optimization was conducted for each of the ten se-  
634 lected models using randomized search with five-fold stratified cross-validation  
635 (`RandomizedSearchCV`). For tree-based ensembles, the search space included the  
636 number of trees, maximum depth, minimum samples per split and leaf, and the  
637 fraction of features considered at each split. For boosting methods, key hyper-  
638 parameters such as the number of boosting iterations, learning rate, tree depth,  
639 subsampling rate, and column subsampling rate were tuned. For the MLP, the

640 number and size of hidden layers, learning rate, and  $L_2$  regularization strength  
641 were varied. In all cases, the primary optimisation criterion was the F1-score of  
642 the chimeric class, averaged across folds.

643 For each model family, the hyperparameter configuration with the highest  
644 mean cross-validation F1-score was selected as the best-tuned estimator. These  
645 tuned models were then refitted on the full training set and evaluated once on the  
646 held-out test set to obtain unbiased estimates of performance. Test-set metrics in-  
647 cluded accuracy, precision, recall, F1-score for the chimeric class, and ROC–AUC.  
648 Confusion matrices and ROC curves were generated for the top-performing mod-  
649 els to characterise common error modes, such as false negatives (missed chimeric  
650 reads) and false positives (clean reads incorrectly labelled as chimeric). The final  
651 model or small set of models for downstream interpretation was chosen based on  
652 a combination of test-set F1-score, ROC–AUC, and practical considerations such  
653 as model complexity and ease of deployment within a bioinformatics pipeline.

### 654 3.1.5 Feature Importance and Interpretation

655 To relate model decisions to biologically meaningful signals, feature-importance  
656 analyses were performed on the best-performing tree-based models. Two comple-  
657 mentary approaches were used. First, built-in importance measures from ensemble  
658 methods (e.g., split-based importances in Random Forest and Gradient Boosting)  
659 were examined to obtain an initial ranking of features based on their contribution  
660 to reducing impurity. Second, model-agnostic permutation importance was com-  
661 puted on the test set by repeatedly permuting each feature column while keeping  
662 all others fixed and measuring the resulting decrease in F1-score. Features whose

663 permutation led to a larger performance drop were interpreted as more influential  
664 for chimera detection.

665 For interpretability, individual features were grouped into four conceptual  
666 families: (i) supplementary alignment and alignment-structure features (e.g., SA  
667 count, spacing between alignment segments, strand consistency), (ii) CIGAR-  
668 derived soft-clipping features (e.g., left and right soft-clipped length, total clipped  
669 bases), (iii) k-mer composition discontinuity features (e.g., cosine distance and  
670 Jensen–Shannon divergence between k-mer profiles of read segments), and (iv) mi-  
671 crohomology descriptors (e.g., microhomology length and local GC content around  
672 putative breakpoints). Aggregating permutation importance scores within each  
673 family allowed assessment of which biological signatures contributed most strongly  
674 to the classifier’s performance. This analysis provided a basis for interpreting the  
675 trained models in terms of known mechanisms of PCR-induced template switching  
676 and for identifying which alignment- and sequence-derived cues are most informa-  
677 tive for distinguishing chimeric from clean mitochondrial reads.

### 678 3.1.6 Validation and Testing

679 Validation will involve both internal and external evaluations. Internal valida-  
680 tion was achieved through five-fold cross-validation on the training data to verify  
681 model generalization and reduce variance due to random sampling. External vali-  
682 dation will be achieved through testing on the 20% hold-out dataset derived from  
683 the simulated reads, which will be an unbiased benchmark to evaluate how well  
684 the trained models generalized to unseen data. All feature extraction and pre-  
685 processing steps were performed using the same bioinformatics pipeline to ensure

686 consistency and comparability across validation stages.

687 Comparative evaluation was performed across all candidate algorithms, in-  
688 cluding a trivial dummy classifier, L2-regularized logistic regression, a calibrated  
689 linear SVM, k-nearest neighbours, Gaussian Naïve Bayes, decision-tree ensembles,  
690 gradient boosting methods, and a shallow MLP. This evaluation determined which  
691 models demonstrated the highest predictive performance and computational effi-  
692 ciency under identical data conditions. Their metrics were compared to identify  
693 which algorithms were most suitable for further refinement.

### 694 3.1.7 Documentation

695 Comprehensive documentation was maintained throughout the study to ensure  
696 transparency and reproducibility. All stages of the research, including data gath-  
697 ering, preprocessing, feature extraction, model training, and validation, were sys-  
698 tematically recorded in a `.README` file in the GitHub repository. For each ana-  
699 lytical step, the corresponding parameters, software versions, and command line  
700 scripts were documented to enable exact replication of results.

701 The repository structure followed standard research data management prac-  
702 tices, with clear directories for datasets and scripts. Computational environments  
703 were standardized using Conda, with an environment file (`environment.arm.yml`)  
704 specifying dependencies and package versions to maintain consistency across sys-  
705 tems.

706 For manuscript preparation and supplementary materials, Overleaf (L<sup>A</sup>T<sub>E</sub>X)  
707 was used to produce publication-quality formatting and consistent referencing.

## 708 3.2 Calendar of Activities

709 Table 3.1 presents the project timeline in the form of a Gantt chart, where each  
710 bullet point corresponds to approximately one week of planned activity.

Table 3.1: Timetable of Activities

Activities (2025)	Nov	Dec	Jan	Feb	Mar	Apr	May
Data Collection and Simulation	• • • •						
Bioinformatics Tools Pipeline			• • • •	• • • •			
Machine Learning Development			• •	• • • •	• • • •	• •	
Testing and Validation						• •	• • • •
Documentation	• • • •	• • • •	• • • •	• • • •	• • • •	• • • •	• • • •

# <sup>711</sup> References

- <sup>712</sup> Anderson, S., Bankier, A., Barrell, B., Bruijn, M., Coulson, A., Drouin, J., ...  
<sup>713</sup> Young, I. (1981, 04). Sequence and organization of the human mitochondrial  
<sup>714</sup> genome. *Nature*, *290*, 457-465. doi: 10.1038/290457a0
- <sup>715</sup> Arango, G., Garner, E., Pruden, A., Heath, L., Vikesland, P., & Zhang, L. (2018,  
<sup>716</sup> 02). Deeparg: A deep learning approach for predicting antibiotic resistance  
<sup>717</sup> genes from metagenomic data. *Microbiome*, *6*. doi: 10.1186/s40168-018  
<sup>718</sup> -0401-z
- <sup>719</sup> Bentley, D. R., Balasubramanian, S., Swerdlow, H. P., Smith, G. P., Milton, J.,  
<sup>720</sup> Brown, C. G., ... Smith, A. J. (2008). Accurate whole human genome  
<sup>721</sup> sequencing using reversible terminator chemistry. *Nature*, *456*(7218), 53–  
<sup>722</sup> 59. doi: 10.1038/nature07517
- <sup>723</sup> Boore, J. L. (1999). Animal mitochondrial genomes. *Nucleic Acids Research*,  
<sup>724</sup> *27*(8), 1767–1780. doi: 10.1093/nar/27.8.1767
- <sup>725</sup> Cameron, S. L. (2014). Insect mitochondrial genomics: Implications for evolution  
<sup>726</sup> and phylogeny. *Annual Review of Entomology*, *59*, 95–117. doi: 10.1146/  
<sup>727</sup> annurev-ento-011613-162007
- <sup>728</sup> Dierckxsens, N., Mardulyn, P., & Smits, G. (2017). Novoplasty: de novo assembly  
<sup>729</sup> of organelle genomes from whole genome data. *Nucleic Acids Research*,

- 730            45(4), e18. doi: 10.1093/nar/gkw955
- 731    Edgar, R. C. (2016). Uchime2: improved chimera prediction for amplicon se-  
732        quencing. *bioRxiv*. Retrieved from <https://api.semanticscholar.org/>  
733        CorpusID:88955007
- 734    Edgar, R. C. (n.d.). Uchime in practice. Retrieved from [https://www.drive5.com/usearch/manual7/uchime\\_practical.html](https://www.drive5.com/usearch/manual7/uchime_practical.html)
- 735    Edgar, R. C., Haas, B. J., Clemente, J. C., Quince, C., & Knight, R. (2011).  
736        Uchime improves sensitivity and speed of chimera detection. *Bioinformatics*,  
737        27(16), 2194–2200. doi: 10.1093/bioinformatics/btr381
- 738    Glenn, T. C. (2011). Field guide to next-generation dna sequencers. *Molecular  
739        Ecology Resources*, 11(5), 759–769. doi: 10.1111/j.1755-0998.2011.03024.x
- 740    Gonzalez, J. M., Zimmermann, J., & Saiz-Jimenez, C. (2004, 09). Evalu-  
741        ating putative chimeric sequences from pcr-amplified products. *Bioin-  
742        formatics*, 21(3), 333-337. Retrieved from <https://doi.org/10.1093/bioinformatics/bti008>  
743        doi: 10.1093/bioinformatics/bti008
- 744    Gray, M. W. (2012). Mitochondrial evolution. *Cold Spring Harbor perspectives  
745        in biology*, 4. Retrieved from <https://doi.org/10.1101/cshperspect.a011403>  
746        doi: 10.1101/cshperspect.a011403
- 747    Hahn, C., Bachmann, L., & Chevreux, B. (2013). Reconstructing mitochondrial  
748        genomes directly from genomic next-generation sequencing reads—a baiting  
749        and iterative mapping approach. *Nucleic Acids Research*, 41(13), e129. doi:  
750        10.1093/nar/gkt371
- 751    Jin, J.-J., Yu, W.-B., Yang, J., Song, Y., dePamphilis, C. W., Yi, T.-S., & Li,  
752        D.-Z. (2020). Getorganelle: a fast and versatile toolkit for accurate de  
753        novo assembly of organelle genomes. *Genome Biology*, 21(1), 241. doi:  
754        10.1186/s13059-020-02154-5
- 755

- 756 Judo, M. S. B., Wedel, W. R., & Wilson, B. H. (1998). Stimulation and sup-  
757 pression of pcr-mediated recombination. *Nucleic Acids Research*, *26*(7),  
758 1819–1825. doi: 10.1093/nar/26.7.1819
- 759 Labrador, K., Agmata, A., Palermo, J. D., Ravago-Gotanco, R., & Pante, M. J.  
760 (2021). Mitochondrial dna reveals genetically structured haplogroups of  
761 bali sardinella (sardinella lemuru) in philippine waters. *Regional Studies in*  
762 *Marine Science*, *41*, 101588. doi: 10.1016/j.rsma.2020.101588
- 763 Layer, R., Hall, I., & Quinlan, A. (2014, 10). Lumpy: A probabilistic framework  
764 for structural variant discovery. *Genome Biology*, *15*. doi: 10.1186/gb-2014  
765 -15-6-r84
- 766 Li, H. (2018, 05). Minimap2: pairwise alignment for nucleotide sequences. *Bioin-*  
767 *formatics*, *34*(18), 3094-3100. Retrieved from <https://doi.org/10.1093/bioinformatics/bty191>  
768 doi: 10.1093/bioinformatics/bty191
- 769 Liang, Q., Bible, P. W., Liu, Y., Zou, B., & Wei, L. (2020, 02). Deepmi-  
770 crobes: taxonomic classification for metagenomics with deep learning. *NAR*  
771 *Genomics and Bioinformatics*, *2*(1), lqaa009. Retrieved from <https://doi.org/10.1093/nargab/lqaa009>  
772 doi: 10.1093/nargab/lqaa009
- 773 Metzker, M. L. (2010). Sequencing technologies — the next generation. *Nature*  
774 *Reviews Genetics*, *11*(1), 31–46. doi: 10.1038/nrg2626
- 775 Mysara, M., Saeys, Y., Leys, N., Raes, J., & Monsieurs, P. (2015). Catch,  
776 an ensemble classifier for chimera detection in 16s rrna sequencing stud-  
777 ies. *Applied and Environmental Microbiology*, *81*(5), 1573-1584. Retrieved  
778 from <https://journals.asm.org/doi/abs/10.1128/aem.02896-14> doi:  
779 10.1128/AEM.02896-14
- 780 Qin, Y., Wu, L., Zhang, Q., Wen, C., Nostrand, J. D. V., Ning, D., ... Zhou, J.  
781 (2023). Effects of error, chimera, bias, and gc content on the accuracy of

- 782 amplicon sequencing. *mSystems*, 8(6), e01025-23. Retrieved from <https://journals.asm.org/doi/abs/10.1128/msystems.01025-23> doi: 10.1128/msystems.01025-23
- 783
- 784
- 785 Qiu, X., Wu, L., Huang, H., McDonel, P. E., Palumbo, A. V., Tiedje, J. M., & Zhou, J. (2001). Evaluation of pcr-generated chimeras, mutations, and heteroduplexes with 16s rrna gene-based cloning. *Applied and Environmental Microbiology*, 67(2), 880–887. doi: 10.1128/AEM.67.2.880-887.2001
- 786
- 787
- 788
- 789 Ren, J., Song, K., Deng, C., Ahlgren, N., Fuhrman, J., Li, Y., ... Sun, F. (2020, 01). Identifying viruses from metagenomic data using deep learning. *Quantitative Biology*, 8. doi: 10.1007/s40484-019-0187-4
- 790
- 791
- 792 Rodriguez-Martin, B., Palumbo, E., Marco-Sola, S., Griebel, T., Ribeca, P., Alonso, G., ... Djebali, S. (2017, 01). Chimpipe: Accurate detection of fusion genes and transcription-induced chimeras from rna-seq data. *BMC Genomics*, 18. doi: 10.1186/s12864-016-3404-9
- 793
- 794
- 795
- 796 Rognes, T., Flouri, T., Nichols, B., Quince, C., & Mahé, F. (2016). Vsearch: a versatile open source tool for metagenomics. *PeerJ*, 4, e2584. doi: 10.7717/peerj.2584
- 797
- 798
- 799 Sedlazeck, F., Rescheneder, P., Smolka, M., Fang, H., Nattestad, M., von Haeseler, A., & Schatz, M. (2018, 06). Accurate detection of complex structural variations using single-molecule sequencing. *Nature Methods*, 15. doi: 10.1038/s41592-018-0001-7
- 800
- 801
- 802
- 803 Sfeir, A., & Symington, L. S. (2015). Microhomology-mediated end joining: A back-up survival mechanism or dedicated pathway? *Trends in Biochemical Sciences*, 40(11), 701-714. Retrieved from <https://www.sciencedirect.com/science/article/pii/S0968000415001589> doi: <https://doi.org/10.1016/j.tibs.2015.08.006>
- 804
- 805
- 806
- 807

- 808 Vervier, K., Mahé, P., Tournoud, M., Veyrieras, J.-B., & Vert, J.-P. (2015,  
809 11). Large-scale machine learning for metagenomics sequence classifica-  
810 tion. *Bioinformatics*, 32(7), 1023-1032. Retrieved from <https://doi.org/10.1093/bioinformatics/btv683>  
811 doi: 10.1093/bioinformatics/btv683
- 812 Willette, D., Bognot, E., Mutia, M. T., & Santos, M. (2011). *Biology and ecology*  
813 *of sardines in the philippines: A review* (Vol. 13; Tech. Rep. No. 1). NFRDI  
814 Technical Paper Series. Retrieved from <https://nfrdi.da.gov.ph/tpjf/etc/Willette%20et%20al.%20Sardines%20Review.pdf>
- 815